IEEE Access
Multidisciplinary | Rapid Review | Open Access Journal

Received February 10, 2020, accepted March 2, 2020, date of publication March 6, 2020, date of current version March 17, 2020.

Digital Object Identifier 10.1109/ACCESS.2020.2978929

Closed-Loop Control for Trajectory Tracking of a Microparticle Based on Input-to-State Stability Through an Electromagnetic Manipulation System

WEICHENG MA[1], MIN XU[1], ZHIXIONG ZHONG[2], XIANGPENG LI[3,4], AND ZHIJIE HUAN[1]

[1]School of Electrical Engineering and Automation, Xiamen University of Technology, Xiamen 361024, China
[2]Fujian Provincial Key Laboratory of Information Processing and Intelligent Control, Minjiang University, Fuzhou 350108, China
[3]College of Mechanical and Electrical Engineering, Soochow University, Suzhou 215000, China
[4]State Key Laboratory of Applied Optics, Changchun Institute of Optics, Changchun 130033, China

Corresponding author: Zhijie Huan (hzjxb@mail.ustc.edu.cn)

This work was supported in part by the National Natural Science Foundation of China under Grant 61903315 and Grant 61873339, in part by the China Postdoctoral Science Foundation under Grant 2016M590497, in part by the Scientific Research Projects for Overseas Students in Xiamen, in part by the Government Guiding Regional Science and Technology Development under Grant 2019L3009, in part by the Natural Science Foundation of Fujian Province under Grant 2019J01869 and Grant 2019J05124, in part by the Promotion Scientific Research Project Young Teachers under Grant XPDKQ18018 and Grant XPDKQ18017, and in part by the Advanced Research Program of Minjiang University under Grant K-30404307 and Grant K-3040610103.

ABSTRACT Magnetic force-based manipulation has several advantages, including its minimally invasive feature and insensitivity to biological substances. Consequently, it has exhibited considerable potential in many medical applications, such as targeted delivery in precise medicine, in which microparticles are driven to the desired regions precisely in vivo. This study investigates an automated and accurate delivery of magnetic microparticles using a self-constructed electromagnetic coil system. After establishing a simplified second-order dynamic model of microparticles suspended in a fluidic environment, a visual-based automated controller that incorporates the concept of input-to-state stability (ISS) into fault-tolerant technique is developed. This controller enables microparticles to follow a desired trajectory under model uncertainties and environmental disturbances, and address the problem that the actual magnetic driving force may not reach the required value due to magnetic loss in the coil system simultaneously. Input constraint of the magnetic force provided by the system due to device capability is also considered in the fault-tolerant ISS-based controller design. Simulation and experimental results are presented to demonstrate the effectiveness of the proposed approach.

INDEX TERMS Automated control, electromagnetic system, magnetic manipulation, microparticles.

I. INTRODUCTION

The accurate delivery of microparticles has recently gained significant attention in precise medicine applications, such as precise targeted drug delivery [1], [2]. Manipulating microparticles to reach desired positions is the key to the success of this procedure. Various microparticle manipulation approaches have been developed; these approaches utilize different techniques, including dielectrophoresis [3]–[6], optical tweezers [7]–[10], and magnetic tweezers [11]–[14]. Among these techniques, magnetic tweezers offer the unique advantage of providing a minimally invasive force in vivo. Moreover, this technique is generally insensitive to most nonmagnetic substances, such as vessels and tissues [15].

In a magnetic micromanipulation system, electromagnetic coils are utilized to produce magnetic forces or torques on magnetic particles. The motion of particles is regulated by controlling the current flowing through electromagnetic coils. In the past several years, researchers have developed various autonomous magnetic manipulation systems and control strategies. A microrobot controlled by a magnetic steering system with a fundamental modeling approach was introduced in [16]; both magnetic and drag properties were tested experimentally in this robot to demonstrate magnetic

The associate editor coordinating the review of this manuscript and approving it for publication was Nasim Ullah.

actuation. In [17], a hybrid system with an integrated circuit chip and a microfluidic channel was used to control magnetic particles with a programmable magnetic field. Utilizing complex nonuniform magnetic field, a magnetic manipulation system was designed in [18] to provide wireless control for a microrobot with five degrees of freedom. In [19], based on the orientation error, visual servo control of a helical microswimmer activated by magnetic field is achieved, as well as planar path following of a straight line. A fish-like deformable nanoswimmer steered by an oscillating magnetic field is proposed in [20], where travelling-wave motion of the nanoswimmer with high speed is achieved. In [21], through magnetic dipole-dipole interaction, a microdimer surface walker formed by two magnetic janus microspheres is design, which is then propelled by oscillating magnetic field to perform back and forth motion.

During manipulation with magnetic tweezers, some environmental disturbances such as system vibrations and temperature gradient-induced flow etc. will significantly degrade motion performance in driving magnetic microparticles, since these manipulated microparticles exhibit high sensitivity to environmental variables at the microscale. Most existing approaches have failed to address this problem in closed-loop control. In [22], a methodology was presented to estimate uncertainties in both force and localization of the microrobots and proposed a robust H_∞ controller using the DK-iteration method to suppress the effect of uncertainties, experiment in a prototype electromagnetic control system has been demonstrated that the H_∞ controller can provably respect the performance measures under higher uncertainties than the PID controller. In [23], a control scheme that compensated disturbance force input to achieve stable dynamics in the entire system was developed. In [24], a microrobot that immersed in fluid and rolling on a surface was controlled by a model predictive controller, which took microrobot nonholonomic property, actuation system limitation and environmental disturbances into account. Given that model uncertainties and environmental disturbances exist ubiquitously, developing a control approach that can manage diverse uncertainties and disturbances is necessary.

In this study, a manipulation control scheme that incorporates ''input-to-state stability'' (ISS) theory [25] is developed to achieve a robust automated control for trajectory tracking of magnetic microparticles actuated by an electromagnetic coil system. According to ISS theory, the bounded disturbances of a nonlinear system can be suppressed to reach the bounded states; thus, the entire system is definitely robust. Assuming that the environmental disturbances are bounded, a conditional robust control technology is incorporated into a backstepping control scheme such that the controlled system can satisfy ISS. This method differs from existing robust control schemes because all the information on uncertainties and disturbances, which are difficult to predict in practice, are not required in the controller design. This idea was initiated in the previous report [26], where a nonlinear observer with a higher gain to suppress estimation error and a lower gain to reduce the steady-state error for manipulation of a microparticle. Through incorporating the ISS-based control approach into the proposed nonlinear observer, the control scheme can guarantee the stability of the entire system. In this paper, we introduce the fault-tolerant technique into the ISS-based controller for dealing with the insufficiency in the magnetic field generation.

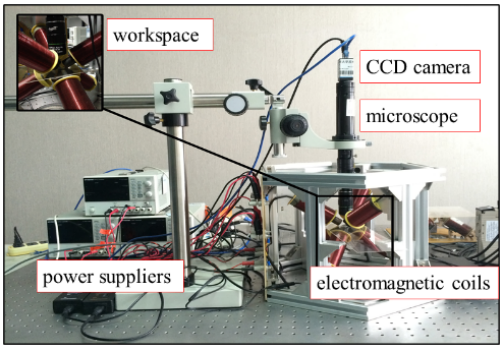

FIGURE 1. Electromagnetic manipulation prototype system.

Since the cores of magnetic coils are made of ferromagnetic materials, magnetic hysteresis loss exists during the re-magnetization process, which causes increase of temperature of the device and hence affects the modelling precision of magnetic field. Further, the magnetic field is dynamic during manipulation, and the modeled magnetic field distribution with numerical simulation is regarded to be quasi-static. The increase of wire resistance varies with the current and manipulation time, which also produces influence on the magnetic field generation. To address all these imperative problems, the fault-tolerant technique is further incorporated into the proposed ISS control scheme in this paper. Subject to the limited capability of generated magnetic force provided by a certain electromagnetic system, input constraint is also discussed in the controller design of this paper. The input-to-state stability of the integrated controller is demonstrated.

II. MODELS

A. ELECTROMAGNETIC MANIPULATION SYSTEM

As shown in Figure 1, a self-constructed electromagnetic coil system developed in USTC-CityU United Center in Suzhou, provides a cubic magnetic workspace with an area of 28 mm $\times$ 28 mm $\times$ 28 mm, which is generated by six orthogonally aligned identical DT4E-core electromagnetic coils. DT4E is a soft magnetic material that exhibits nonlinear isotropy. Consequently, reaching saturation is difficult for the electromagnetic coils because the magnetic resistance of the cores is low whereas air gap is high. Thus, the cores always work at a linear stage of their B–H curves. Three identical DC power suppliers (model no. GWINSTEK GPD 3303S), each with two output channels, are connected to the six coils. The power supply has a maximum current of 3A and a minimum response time of 30ms. As real-time visual feedback of the controlled beads is obtained, a control signal is set to the power supply in order to set the desired DC current.

The current of the power supply flows into the coils. Thus, the coils and the cores induce a corresponding magnetic field. Superimposing the magnetic field generated by the six coils produces the resultant magnetic field. This electromagnetic coil system can generate a maximum magnetic field of 50 mT and a maximum gradient of 2 T/m, which is below the recommended maximum safety field strength of 4T. In the previous work [27], a magnetic field distribution model was established by using the finite element method (FEM). The coil parameters are set as follows: coil length is 76 mm, coil diameter is 25 mm, and number of turns is 576. A slide that contains a microparticle (or bead) is placed at the center of the workspace. During the experiment, the microbead, which is controlled by the electromagnetic coils, moves in a 3D direction. Using a DFK274 CCD camera with a resolution of 1600 × 1200 pixels and the sampling frequency of 20fps, bead motion can be visually guided from the top view. The resolution of the measured position is 0.15 μm/pixel. The control software of the experimental setup is developed using C++ program with an Intel Core i3 Duo 3.0 GHZ processor running in Windows XP.

The architecture of the closed-loop control is illustrated as follows. The desired trajectory of the microbead is initially provided using a software interface. During the motion, bead position can be detected through image processing. With real-time position feedback, coil current can be generated based on the proposed control algorithm, which is set in the power supply to generate the corresponding magnetic force. Hence, the bead can be automatically manipulated to track the desired trajectory and move toward the final destination. The sampling time for the controller is set as 50 ms in the system.

The magnetically driven microparticles are made of either ferromagnetic materials [28] or superparamagnetic materials [29], [30]. Ferromagnetic materials exhibit high susceptibility and saturation magnetization, thus requiring small magnetic field and field gradient of the manipulation system. However, ferromagnetic materials maintain magnetization once the particle is magnetized, and the magnetization even exists after the magnetic field vanishes. This unavoidable hysteresis effect causes a difficulty in controlling the magnetic moment of a microparticle, and subsequently, results in unexpected interactions among the magnetized particles. When the size of ferromagnetic particles is smaller than a critical value, ferromagnetism turns to superparamagnetism and the materials exhibit no coercivity. Superparamagnetic materials, although with lower susceptibility, do not have hysteresis. The superparamagnetic material was therefore employed in this study so that minimal negative effect on the organisms was produced after the external magnetic field vanished. Figure 2 illustrates the microbeads used in this study, where the beads are filled with Fe_3O_4 nanoparticles and coated with hydrophilic agarose polymer (purchased from Suzhou Knowledge & Benefit Sphere Tech. Co., Ltd). Table 1 presents the design parameters of the microbead used in this study.

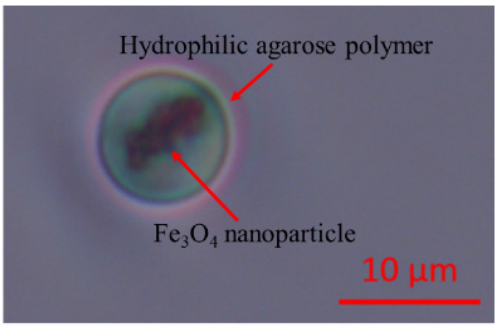

FIGURE 2. Microbead used in the experiment.

TABLE 1. Designed parameters of the microbead.

Parameters	Values	Units
Density (ρ_m)	1.1	g / cm^3
Radius (R)	5	μm
Susceptibility (χ)	0.02	-

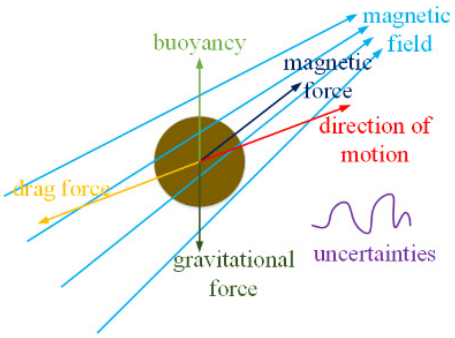

FIGURE 3. External forces exerted on the microbead in the electromagnetic field.

B. DYNAMICS

After the microparticle flows into the slide via syringing, it moves with the fluidic flow in a 3D direction. Since the research objective of this study is to manipulate the microparticle to track the desired trajectory, only the dynamic translational motion of the particle, driven by the magnetic force exerted by the magnetic field gradient, was investigated in this paper. To simplify the problem, all the manipulated microparticles are considered to have a spherical shape. Figure 3 illustrates the forces exerted on the microparticle as it moves in the electromagnetic field, including magnetic force, drag, buoyancy, and gravitational force.

The magnetic force exerted on the microbead is defined as follows [15]:

$$\boldsymbol{F_m} = V_m \frac{\Delta\chi}{\mu_0} (\boldsymbol{B} \cdot \nabla) \boldsymbol{B} \tag{1}$$

where μ_0 is the magnetic permeability of free space and defined as $4\pi \times 10^{-7}$Tm/A, $\mathbf{B}$ is the magnetic flux density with the unit Tesla (T), and ∇ is a gradient operator, V_m is

the volume of the magnetized object, $\Delta\chi = \chi_m - \chi_w$ is the effective susceptibility of the particle relative to the medium.

For a given microbead, the magnetic force exerted on it is a function of both coil current combination $\mathbf{I}$ and bead position $\mathbf{r}$ based on the Biot–Savart law. Keeping the magnetic field value unchanged, the magnetic force on the microparticle is controlled by changing the field gradient. Thus, magnetic force can be simplified as a linear function of current $\mathbf{I}$ to reduce computational load, and Eq. (1) can be rewritten as follows:

$$\boldsymbol{F_m} = f(\boldsymbol{I}) \tag{2}$$

The coil current combination $\mathbf{I}$ for the corresponding magnetic force $\mathbf{F_m}$ can be obtained through the pseudoinverse of f.

The drag force caused by the fluidic environment to the small particle is [16]

$$\boldsymbol{F_d} = C_d \rho_f A \boldsymbol{v}^2/2 \tag{3}$$

where C_d is the drag coefficient that represents the overall effect of the particle geometry on the drag force, which is a function of the Reynolds number Re; ρ_f is the fluid density; A is the cross-sectional area of the particle; and $\boldsymbol{v}$ is the relative velocity of the particle with respect to the fluid medium. Considering that the fluid used in the experiment is stationary water, $\boldsymbol{v}$ can be simplified as the velocity of the microbead.

The microbead used in this study is spherical, the Reynolds number value of the fluid is less than 10^{-3}, which indicates that the flow is a laminar flow with low Reynolds number. Thus, the drag force can be simplified as follows:

$$\boldsymbol{F_d} = 6\pi\eta R\boldsymbol{v} \tag{4}$$

where R is the bead radius, and η is the dynamic viscosity of the fluid. This equation is known as Stokes drag. Given that the fluid used in this study is lightly salted water, the dynamic viscosity is approximated as 1×10^{-3} Pa.s. Since the fluid density is similar to that of the manipulated microbead, the buoyancy counteracts the gravitational force. As a result, both buoyancy and gravitational forces can be neglected and this study can be simplified in 2D.

As analyzed before, the magnetic force may not reach the required value in practice, define $\varepsilon\epsilon$ (0, 1] as the fault gain [31], where $0 < \varepsilon \leq 1$, and replace $\mathbf{F_m}$ by $\boldsymbol{F'}_m = \varepsilon \boldsymbol{F}_m$. On the basis of the aforementioned analysis, the dynamic equation of the microbead suspended in fluid can be derived as follows:

$$\mathrm{m}\cdot\frac{d^2\boldsymbol{r}}{dt^2} = \boldsymbol{F'}_m - \boldsymbol{F_d} + \boldsymbol{\Delta} \tag{5}$$

where m denotes the bead mass, $\boldsymbol{r}$ is the bead position, and Δ is the unknown bounded parameter to subsume various uncertainties and environmental disturbances. The disturbances may include magnetic field noise, influences of other particles in the environment, hydrodynamics, thermodynamics and other microenvironment disturbances.

III. CONTROL

Once the desired trajectory is provided as a function of time, the desired signals for position and velocity of any time can be obtained according to the trajectory function. Let $\boldsymbol{r_d}$ be the desired position of the bead and $\boldsymbol{r_0}$ be the actual position observed through the CCD camera. The position tracking error is defined as $\boldsymbol{e} = \boldsymbol{r_0} - \boldsymbol{r_d}$, and the velocity tracking error is defined as $\dot{\boldsymbol{e}} = \dot{\boldsymbol{r}}_0 - \dot{\boldsymbol{r}}_d$. The objective of this work is to design an appropriate controller that enables a microbead to follow a desired trajectory accurately, such that both position and velocity trajectory tracking errors $\{\boldsymbol{e}, \dot{\boldsymbol{e}}\} \rightarrow 0$ when time $t \rightarrow \infty$.

A transformation function is introduced as $\mathbf{z_1} = \mathbf{e}$, $\mathbf{z_2} = \mathrm{d}\mathbf{e}/\mathrm{d}t$. As mentioned earlier, $\boldsymbol{v}$ in Eq. (4) can be simplified as the particle velocity when the fluid is static. Hence, it can be replaced by $\mathrm{d}\mathbf{r_0}/\mathrm{d}t$. Define $a = -6\pi\eta R/\mathrm{m}$, $b = 1/m$, and $c = -6\pi\eta \mathrm{R}\dot{\boldsymbol{r}}_d/m - \ddot{\boldsymbol{r}}_d$. The magnetic force $\mathbf{F_m}$ is regarded as the system input. The unknown uncertainty Δ/m can be simplified as Δ. Hence, system (5) can be transformed into the following equivalent system:

$$\begin{cases} \dot{\boldsymbol{z}}_1 = \boldsymbol{z}_2 \\ \dot{\boldsymbol{z}}_2 = a\boldsymbol{z}_2 + b\varepsilon\boldsymbol{F_m} + c + \Delta \end{cases} \tag{6}$$

where $\varepsilon \in (0, 1]$ denotes the fault gain, and $\mathbf{F_m}$ is control input.

With the null tracking error $\mathbf{z_1}$ and the derivative of this error $\mathbf{z_2}$, the microbead can successfully follow the desired trajectory. Subsequently, we develop a controller to achieve the desired magnetic force $\mathbf{F_m}$, which can enable the controlled system (6) to satisfy ISS. Coil current combination $\mathbf{I}$ is then calculated based on $\mathbf{F_m}$.

A. FAULT-TOLERANT ISS-BASED BACKSTEPPING CONTROLLER

To manage the practical problem of actuator error, the fault-tolerant technique is incorporated into the previous ISS-based [26] controller design. Using recursive application of backstepping [32], the fault-tolerant ISS-based controller is designed as

$$\boldsymbol{F_m} = -\frac{1}{b\mu}\left(\left|\left(1 - ak_1 - k_1^2\right)\boldsymbol{z_1} + c\right| sgn\left(\tilde{\boldsymbol{z}}_2\right) + \left(\left|a + k_1 + \frac{1}{2\delta^2}\right| + k_2\right)\tilde{\boldsymbol{z}}_2\right) \tag{7}$$

where $\tilde{\boldsymbol{z}}_2 = \boldsymbol{z}_2 + k_1\boldsymbol{z_1}$, $0 < \mu \leq \varepsilon$, μ is the insufficient coefficient, k_1, k_2 and δ are positive control gains, $sgn\left(\tilde{\boldsymbol{z}}_2\right)$ is a signal function expressed as

$$sgn\left(\tilde{\boldsymbol{z}}_2\right) = \begin{cases} 1 & \tilde{\boldsymbol{z}}_2 > 0 \\ 0 & \tilde{\boldsymbol{z}}_2 = 0 \\ -1 & \tilde{\boldsymbol{z}}_2 < 0 \end{cases} \tag{8}$$

Theorem: Considering the closed-loop system (6), the fault-tolerant controller (7) guarantees the input-to-state stability of $\boldsymbol{z_1}$ and $\tilde{\boldsymbol{z}}_2$ in presence of insufficiency of magnetic force $\boldsymbol{F_m}$. That is, through adjusting the control gains k_1, k_2, δ and μ, the position error $\boldsymbol{z_1}$ and the velocity error $\tilde{\boldsymbol{z}}_2$ can be retained in a small neighborhood of zero with existence of the

uncertainty Δ. *Furthermore, if the uncertainty* Δ *vanishes, both* z_1 *and* $\tilde{z}_2$ *converge to zero.*

Proof: Define the Lyapunov function candidate as

$$V = z_1^2/2 + \tilde{z}_2^2/2 \tag{9}$$

Its first-order differentiation, referring to the updated dynamic system (6), is

$$\dot{V} = -k_1 z_1^2 + \tilde{z}_2 \left(\left(1 - ak_1 - k_1^2\right) z_1 + (a + k_1)\tilde{z}_2 + c + b\varepsilon \boldsymbol{F_m} \right) + \Delta . \tilde{z}_2 \tag{10}$$

Substituting the inequality $\Delta . \tilde{z}_2 \leq \frac{\delta^2}{2}\Delta^2 + \frac{\tilde{z}^2}{2\delta^2}$ (δÂčÂ¿0) into (10), Eq. (10) becomes

$$\begin{aligned} \dot{V} &\leq -k_1 z_1^2 + \frac{\delta^2\Delta^2}{2} + \tilde{z}_2 \left(\left(1 - ak_1 - k_1^2\right) z_1 \right. \\ &\quad \left. + c + \left(a + k_1 + 1/2\delta^2\right)\tilde{z}_2 + b\varepsilon \boldsymbol{F_m} \right) \\ &\leq -k_1 z_1^2 + \frac{\delta^2\Delta^2}{2} + b\varepsilon \boldsymbol{F_m}\tilde{z}_2 + \left| \left(1 - ak_1 - k_1^2\right) z_1 \right| \\ &\quad + c\,|\tilde{z}_2| + \left| a + k_1 + \frac{1}{2\delta^2} \right| \tilde{z}_2^2 \end{aligned} \tag{11}$$

Substituting $\mathbf{F}_m$ in (7) into (11) yields

$$\begin{aligned} \dot{V} &\leq -k_1 z_1^2 + \frac{\delta^2\Delta^2}{2} - \frac{\varepsilon}{\mu} \left(\frac{\left|\left(1 - ak_1 - k_1^2\right) z_1 + c\right|}{|\tilde{z}_2|} \tilde{z}_2^2 \right. \\ &\quad \left. + \left(\left| a + k_1 + \frac{1}{2\delta^2} \right| + k_2 \right) \tilde{z}_2^2 \right) + \\ &\quad + \frac{\left|\left(1 - ak_1 - k_1^2\right) z_1 + c\right|}{|\tilde{z}_2|} \tilde{z}_2^2 + \left(\left| a + k_1 + \frac{1}{2\delta^2} \right| \right) \tilde{z}_2^2 \\ &= -k_1 z_1^2 - \frac{\varepsilon k_2 \tilde{z}_2^2}{\mu} + \frac{\delta^2\Delta^2}{2} + \left(1 - \frac{\varepsilon}{\mu}\right) \\ &\quad \times \left(\frac{\left|\left(1 - ak_1 - k_1^2\right) z_1 + c\right|}{|\tilde{z}_2|} + \left| a + k_1 + \frac{1}{2\delta^2} \right| \right) \tilde{z}_2^2 \end{aligned} \tag{12}$$

Since $0 < \mu \leq \varepsilon$, $1 - \varepsilon/\mu \leq 0$. Eq. (12) becomes

$$\dot{V} \leq -k_1 z_1^2 - k_2 \tilde{z}_2^2 + \delta^2\Delta^2/2 \tag{13}$$

Let $K = \min\{k_1, k_2\}$, Eq. (13) becomes

$$\dot{V} \leq -2KV + \delta^2\Delta^2/2 \tag{14}$$

By multiplying both sides of Eq. (14) with e^{2Kt} with further integration over [0,t], Eq. (14) becomes

$$\begin{aligned} V(t) &\leq -e^{-2Kt} V(0) + \frac{\delta^2}{2} \int_0^t e^{-2K(t-\tau)} \boldsymbol{\Delta}^2 d\tau \\ &\leq -e^{-2Kt} V(0) + \frac{\delta^2}{2} \frac{1 - e^{-2Kt}}{2K} \sup_{0 \leq \tau \leq t} \boldsymbol{\Delta}^2 \end{aligned} \tag{15}$$

By taking the square root and substituting Lyapunov function (9) into Eq. (15), the following inequality is obtained

$$\left\| \begin{matrix} z_1(t) \\ \tilde{z}_2(t) \end{matrix} \right\| \leq e^{-Kt} \left\| \begin{matrix} z_1(0) \\ \tilde{z}_2(0) \end{matrix} \right\| + \frac{\delta}{2} \sqrt{\frac{1 - e^{-2Kt}}{K}} \sup_{0 \leq \tau \leq t} \boldsymbol{\Delta}. \tag{16}$$

Eq. (16) is in the form of ISS. According to ISS theory, for any bounded input, which is regarded as uncertainties Δ in the system, the state x(t) is bounded. Furthermore, with a zero input u(t), the system is uniformly asymptotically stable. Hence, it is proved that the input-to-state stability of z_1 and $\tilde{z}_2$ while considering insufficient force generation. As seen in Eq. (14), small δ, μ or large k_i ($i = 1,2$) are needed to maintain $\|z_1\|$ and $\|\tilde{z_2}\|$ within the desired domain. The magnitudes of the disturbances and uncertainties also affect the control parameter δ. That is, a large control energy is needed to suppress uncertainties.

B. STABILITY ANALYSIS UNDER INPUT CONSTRAINT

Since the actual magnetic force provided by a certain electromagnetic system is limited, a saturation function for the proposed controller (7) is further introduced to manage the case of input constraint and analyze the stability of the system under input constraint.

The fault-tolerant ISS based controller with saturation function is modified as

$$\tilde{F}_m = Sat_N(\boldsymbol{F_m}) \tag{17}$$

where

$$Sat_N(\boldsymbol{F_m}) = \begin{cases} N & if\ |\boldsymbol{F_m}| \geq N \\ \boldsymbol{F_m} & if\ |\boldsymbol{F_m}| \leq N \end{cases} \tag{18}$$

Now the fault-tolerant ISS-based controller with input constraint can also guarantee ISS is shown.

Define the same Lyapunov function candidate as in Sec. III-A. In a similar manner, the following inequality is obtained

$$\begin{aligned} \dot{V} &\leq -k_1 z_1^2 + \left(a + k_1 + \frac{1}{2\delta^2} \right) \tilde{z}_2^2 + z_1 \tilde{z}_2 \left(1 - ak_1 - k_1^2\right) \\ &\quad + \tilde{z}_2 \left(c + b\varepsilon \tilde{F}_m \right) + \frac{\delta^2\Delta^2}{2} \\ &\leq -k_1 z_1^2 + \left(a + k_1 + \frac{1}{2\delta^2} \right) \tilde{z}_2^2 + \left(1 - ak_1 - k_1^2\right) |z_1|\,|\tilde{z}_2| \\ &\quad + |c + b\varepsilon N \cdot \mathrm{sgn}(\boldsymbol{F_m})| \cdot |\tilde{z}_2| + \frac{\delta^2\Delta^2}{2}. \end{aligned} \tag{19}$$

Assume that $1 - ak_1 - k_1^2 > 0$ and $|z_1| \leq \frac{\varpi}{1 - ak_1 - k_1^2}$, Eq. (19) becomes

$$\begin{aligned} \dot{V} \leq -k_1 z_1^2 + \left(a + k_1 + \frac{1}{2\delta^2} \right) \tilde{z}_2^2 + (\varpi + |c + b\varepsilon N \mathrm{sgn}(\boldsymbol{F_m})|) \\ \times |\tilde{z}_2| + \frac{\delta^2\Delta^2}{2}. \end{aligned} \tag{20}$$

Let $1 < \alpha < -\frac{a + 1/2\delta^2}{k_1}$ and $\eta = \varpi + |c + b\varepsilon N \cdot sgn(\boldsymbol{F_m})|$. Eq. (20) becomes

$$\begin{aligned} \dot{V} &\leq -k_1 z_1^2 + \left(a + \alpha k_1 + \frac{1}{2\delta^2} \right) \tilde{z}_2^2 \\ &\quad - \left((\alpha - 1) k_1 \tilde{z}_2^2 + \eta\,|\tilde{z}_2| + \beta^2 \right) + \beta^2 + \frac{\delta^2\Delta^2}{2} \\ &\leq -k_1 z_1^2 + \left(a + \alpha k_1 + \frac{1}{2\delta^2} \right) \tilde{z}_2^2 + \beta^2 + \frac{\delta^2\Delta^2}{2}. \end{aligned} \tag{21}$$

where $\beta = \eta / \sqrt{4(\alpha - 1)k_1}$.

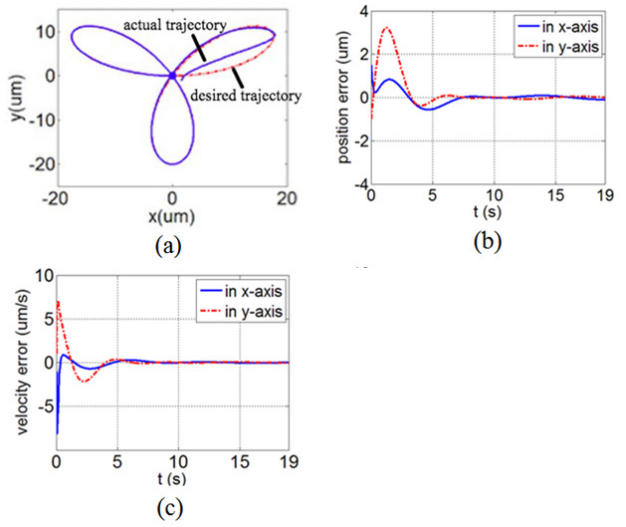

FIGURE 4. First simulation: (a) trajectory tracking of the bead with the standard ISS-based controller; (b) position tracking error; (c) velocity tracking error.

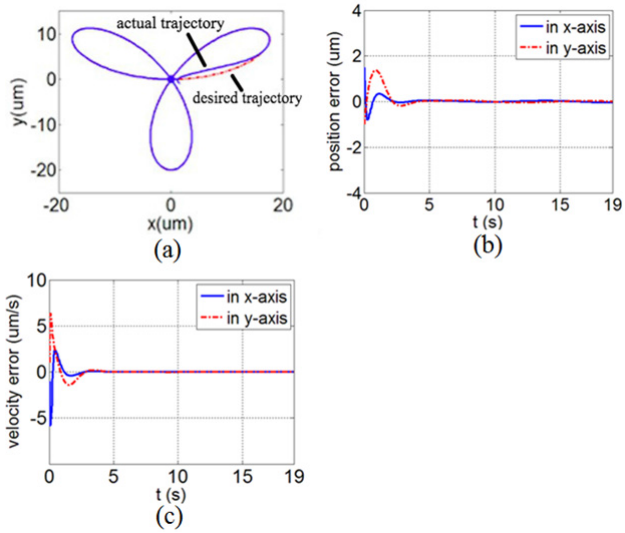

FIGURE 5. Second simulation: (a) trajectory tracking of the bead with the fault-tolerant ISS-based controller with input constraint; (b) position tracking error; (c) velocity tracking error.

Define a positive parameter $\tilde{k}_2 = -\mathrm{a}-\alpha k_1 - \frac{1}{2\delta^2}$. Finally yields the following inequality

$$\dot{V} \leq -k_1 z_1^2 - \tilde{k}_2 \tilde{z}_2^2 + \beta^2 + \frac{\delta^2 \Delta^2}{2}. \tag{22}$$

which can be also proved to be ISS.

IV. SIMULATIONS

Numerical simulations were performed to verify the proposed control approach. The parameters of the bead were set as m $= 3.351 \times 10^{-11}$kg, $\eta = 10^{-3}$Pa.s. The bead was driven to follow a 2D clover-like curve, assuming that the fault gain was $\varepsilon = 0.6+0.1\,sin(t)$. The desired trajectory was specified as

$$\begin{cases} x_d = 20\ sin\ (t/2)\ cos\ (t/6)\ \mu m \\ y_d = 20\ sin\ (t/2)\ sin\ (t/6)\ \mu m \end{cases} \tag{23}$$

Using the oscillation observation technology [7], a sine function is introduced to simulate the sudden vibrations and a normal distribution noise is introduced to simulate random microenvironment disturbances. Hence, the unknown bounded parameter Δ was modeled as follows

$$\begin{cases} \Delta_x = 2\ sin\ (t) + B\ \mu m \\ \Delta_y = 6\ sin\ (0.5t) + B\ \mu m \end{cases} \tag{24}$$

where B was a normal distribution noise with a mean of zero and a standard deviation of 0.2. The control coefficients were set as $k_1 = k_2 = 15$, and $\delta = 0.8$.

In the first simulation, the bead was driven to track along the clover-like trajectory under the standard ISS-based controller [26]. Figure 4(a) shows the simulation that the microbead could successfully track desired trajectory. The control performance, as shown in Figures 4(b–c), indicates that both position and velocity tracking errors converged into a small neighborhood of origin in less than 10 seconds.

In the second simulation, the bead was required to move along the same clover-like curve but controlled by the fault-tolerant ISS-based controller with input constraint (17), where the insufficient coefficient was chosen as $\mu = 0.5$ and the saturation value N=10. The control coefficients were the same as in the first simulation, namely, $k_1 = k_2 = 15$, and $\delta = 0.8$. Figure 5(a) shows the simulation of the trajectory tracking process of the bead in the second simulation. It is seen that the bead could follow the desired clover-like trajectory in less than 5 seconds. Figures 5(b–c) illustrate that both the position and velocity tracking errors converged rapidly into a small neighborhood of the origin.

The aforementioned simulation results successfully demonstrated that the proposed ISS-based backstepping controller could enable the microbead to follow a desired trajectory precisely even under model uncertainties and environmental disturbances. With the proposed fault-tolerant ISS-based controller with input constraint, the bead exhibited better tracking performance than that under the standard ISS-based controller. Furthermore, the steady-state error under the fault-tolerant control was smaller.

V. EXPERIMENTS

The experiments were performed on the self-constructed electromagnetic system illustrated in Figure 1. Both the standard ISS-based controller and the fault-tolerant ISS-based controller were implemented.

Figure 6 illustrates the architecture of the control strategy. The desired trajectory of the microbead is initially provided using a software interface. During the motion, bead position can be detected through image processing. With real-time position feedback, coil current can be generated based on the proposed control algorithm, which is set in the power supplier to generate the corresponding magnetic force. Hence, the bead can be automatically manipulated to track the desired trajectory and move toward the final destination.

In the first experiment, the bead was driven to move along a Bernoulli curve under the standard ISS-based control law.

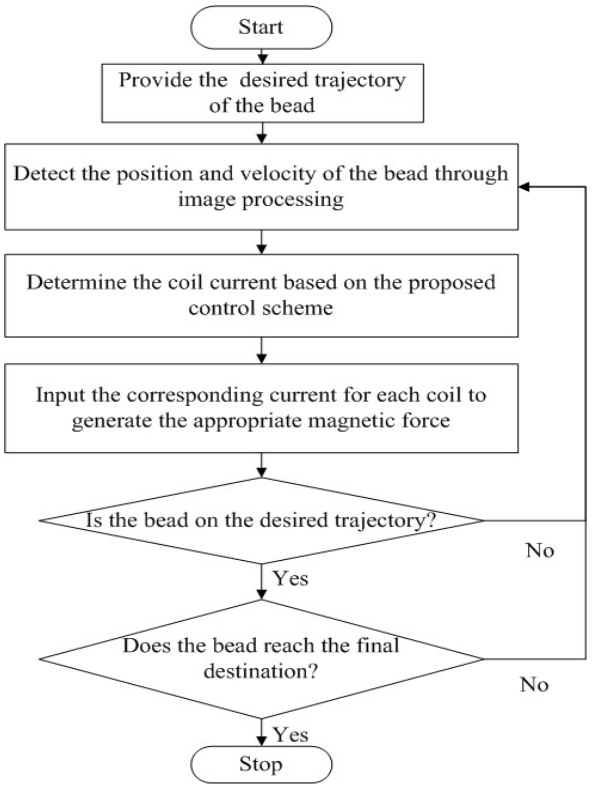

FIGURE 6. Block diagram of global system.

The control parameters were set as $k_1 = k_2 = 20$, and $\delta = 5$. Figure 7(a) illustrates the experimental results of the trajectory tracking process of the bead. In the experiment, the system suffered from numerous disturbances because of various reasons. Examples of these reasons included the influences of other particles in the environment on the magnetic field perturbed the motion of the bead. Hydrodynamics, thermodynamics and environmental uncertainties caused various disturbances to the motion control of the bead. The results presented in Figure 7(a) demonstrated that the proposed ISS-based robust controller could overcome these disturbances and enable the bead to track successfully along the given trajectory. Figures 7(b-c) shows that the position tracking error $\mathbf{e}$ was less than 30 μm and the velocity tracking error $\dot{\boldsymbol{e}}$ was less than 10 $\mu m/s$ during the manipulation.

In the second experiment, the bead was controlled to move along the same trajectory, under the fault-tolerant ISS-based controller. The same control parameters as in the first experiment were used, namely, $k_1 = k_2 = 20$, $\delta = 5$ and the insufficient coefficient were chosen as $\mu = 0.6$. The input magnetic force $\mathbf{F_m}$ is limited since the maximum coil current generated by the power supplier is 3A. Figure 8(a) illustrates the experimental results of the trajectory tracking process of the bead in the second experiment. Figure 8(b) shows that the position tracking error $\mathbf{e}$ was less than 20 μm, and Figure 8(c) shows that the velocity tracking error $\dot{\boldsymbol{e}}$ was maintained within a small neighborhood of zero.

A comparative experiment of using traditional PID controller was also performed, in which the bead was driven

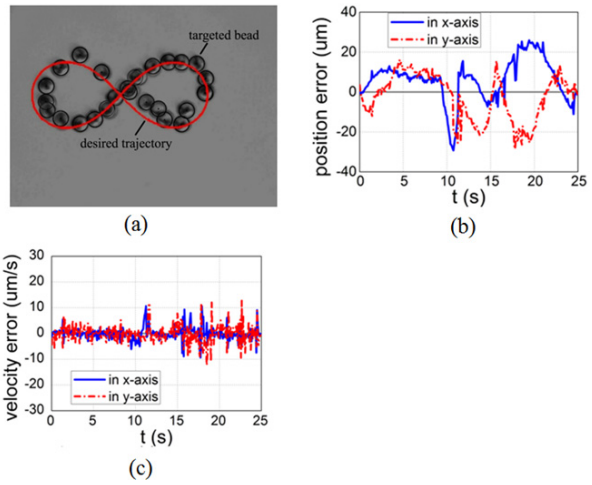

FIGURE 7. First experiment: (a) trajectory tracking process of the bead with the standard ISS-based controller; (b) position tracking error; (c) velocity tracking error.

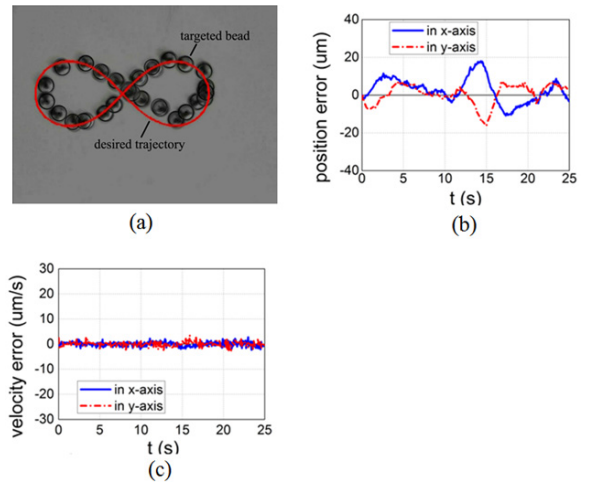

FIGURE 8. Second experiment: (a) trajectory tracking process of the bead with the fault-tolerant ISS-based controller with input constraint; (b) position tracking error; (c) velocity tracking error.

to move along the same Bernoulli curve. The results as shown in Figure 9(a) indicated that under the PID control, the bead could also track the desired trajectory but with poor control performance. Figures 9(b-c) show the position and velocity errors of the bead during manipulation, which are much larger than that under the proposed robust control.

All the above experiments were repeated for at least three times, applied on different magnetic microbeads. Table 2 provides the mean squared errors of randomly selected three experimental trials under the three different control methods.

In conclusion, both the proposed ISS-based controllers could guarantee successful trajectory tracking of a magnetic microparticle driven by an electromagnetic coil system even under system disturbances and uncertainties. Furthermore, the fault-tolerant ISS-based controller could achieve better tracking performance than that under the standard ISS-based controller, even taking the input constraint into account.

TABLE 2. Mean squared tracking errors.

Experiment No.	Control scheme	Position error (μm)		Velocity error (μm/s)	
		x-axis	y-axis	x-axis	y-axis
1	Standard ISS-based	10.43	11.68	2.50	3.79
2		11.26	11.11	2.68	3.39
3		10.96	11.28	2.75	3.57
4	Fault-tolerant ISS-based	6.50	5.26	0.89	1.10
5		6.28	5.87	0.72	1.25
6		6.50	5.37	1.05	1.11
7	PID	17.59	13.64	3.54	3.09
8		17.97	13.25	3.85	3.25
9		16.28	14.10	3.30	3.97

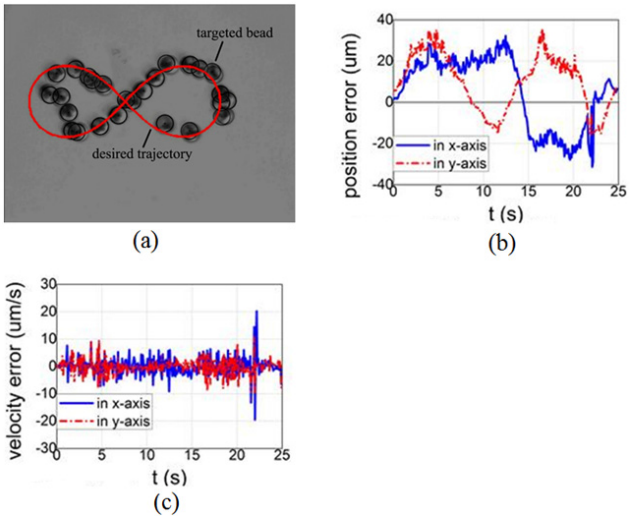

FIGURE 9. Third experiment: trajectory tracking process of the bead with the traditional PID controller; (b) position tracking error; (c) velocity tracking error.

VI. CONCLUSION

A new automated control approach to manipulating magnetic microparticles using an electromagnetic coil system is proposed in this study. The dynamics of a microparticle suspended in a fluidic environment is initially analyzed. To address the problem that the magnetic force acted on the microparticle may not be sufficiently high due to loss of the magnetic field, and that the capability of generated magnetic force is limited, a fault-tolerant ISS-based controller with input constraint is further designed for automatic trajectory tracking under model uncertainties and environmental disturbances. Simulations and experiments are performed in a self-constructed electromagnetic system to demonstrate the effectiveness of the proposed approach. The rotational manipulation with magnetic torque will be further studied in the future work.

ACKNOWLEDGMENT

The authors thank the support and help from Shenzhen Fuxda Electronics Co. Ltd. and the State Key Laboratory of Applied Optics.

REFERENCES

[1] J. Dobson, "Magnetic nanoparticles for drug delivery," *Drug Develop. Res.*, vol. 67, no. 1, pp. 55–60, 2006.
[2] P. J. Cregg, K. Murphy, and A. Mardinoglu, "Inclusion of interactions in mathematical modelling of implant assisted magnetic drug targeting," *Appl. Math. Model.*, vol. 36, no. 1, pp. 1–34, Jan. 2012.
[3] R. Pethig, "Review article-dielectrophoresis: Status of the theory, technology, and applications," *Biomicrofluidics*, vol. 4, no. 3, 2010, Art. no. 039901.
[4] Z. Huan, H. K. Chu, J. Yang, and D. Sun, "Characterization of a honeycomb-like scaffold with dielectrophoresis-based patterning for tissue engineering," *IEEE Trans. Biomed. Eng.*, vol. 64, no. 4, pp. 755–764, Apr. 2017.
[5] Z. Huan, H. K. Chu, H. Liu, J. Yang, and D. Sun, "Engineered bone scaffolds with dielectrophoresis-based patterning using 3D printing," *Biomed. Microdevices*, vol. 19, no. 4, p. 102, Dec. 2017.
[6] Z. Huan, W. Ma, M. Xu, Z. Zhong, X. Li, and Z. Zhu, "Cell patterning via optimized dielectrophoretic force within hexagonal electrodes *in vitro* for skin tissue engineering," *Int. J. Adv. Manuf. Technol.*, vol. 105, no. 12, pp. 4899–4907, Dec. 2019.
[7] H. Chen and D. Sun, "Moving groups of microparticles into array with a Robot–Tweezers manipulation system," *IEEE Trans. Robot.*, vol. 28, no. 5, pp. 1069–1080, Oct. 2012.
[8] M. Xie, A. Shakoor, and C. Wu, "Manipulation of biological cells using a robot-aided optical tweezers system," *Micromachines*, vol. 9, no. 5, p. 245, 2018.
[9] M. Xie, A. Shakoor, C. Li, and D. Sun, "Robust orientation control of multi–DOF cell based on uncertainty and disturbance estimation," *Int. J. Robust Nonlinear Control*, vol. 29, no. 14, pp. 4859–4871, Sep. 2019.
[10] M. Xie, A. Shakoor, Y. Shen, J. K. Mills, and D. Sun, "Out-of-Plane rotation control of biological cells with a robot-tweezers manipulation system for orientation-based cell surgery," *IEEE Trans. Biomed. Eng.*, vol. 66, no. 1, pp. 199–207, Jan. 2019.
[11] E. Diller, S. Floyd, C. Pawashe, and M. Sitti, "Control of multiple heterogeneous magnetic microrobots in two dimensions on nonspecialized surfaces," *IEEE Trans. Robot.*, vol. 28, no. 1, pp. 172–182, Feb. 2012.
[12] J. Li, X. Li, T. Luo, R. Wang, C. Liu, S. Chen, D. Li, J. Yue, S.-H. Cheng, and D. Sun, "Development of a magnetic microrobot for carrying and delivering targeted cells," *Sci. Robot.*, vol. 3, no. 19, Jun. 2018, Art. no. eaat8829.

[13] D. Li, F. Niu, J. Li, X. Li, and D. Sun, "Gradient-enhanced electromagnetic actuation system with a new core shape design for microrobot manipulation," *IEEE Trans. Ind. Electron.*, vol. 67, no. 6, pp. 4700–4710, Jun. 2020, doi: 10.1109/TIE.2019.2928283.
[14] H. Yu, W. Tang, G. Mu, H. Wang, X. Chang, H. Dong, L. Qi, G. Zhang, and T. Li, "Micro-/Nanorobots propelled by oscillating magnetic fields," *Micromachines*, vol. 9, no. 11, p. 540, 2018.
[15] Q. Pankhurst, J. Connolly, S. Jones, and J. Dobson, "Applications of magnetic nanopaticles in biomedine," *J. Phys. D, Appl. Phys.*, vol. 36, pp. R167–R181, Jun. 2003.
[16] K. B. Yesin, K. Vollmers, and B. J. Nelson, "Modeling and control of untethered biomicrorobots in a fluidic environment using electromagnetic fields," *Int. J. Robot. Res.*, vol. 25, nos. 5–6, pp. 527–536, May 2006.
[17] H. Lee, Y. Liu, R. M. Westervelt, and D. Ham, "IC/Microfluidic hybrid system for magnetic manipulation of biological cells," *IEEE J. Solid-State Circuits*, vol. 41, no. 6, pp. 1471–1480, Jun. 2006.
[18] M. P. Kummer, J. J. Abbott, B. E. Kratochvil, R. Borer, A. Sengul, and B. J. Nelson, "OctoMag: An electromagnetic system for 5-DOF wireless micromanipulation," *IEEE Trans. Robot.*, vol. 26, no. 6, pp. 1006–1017, Dec. 2010.
[19] T. Xu, G. Hwang, N. Andreff, and S. Regnier, "Planar path following of 3-D steering scaled-up helical microswimmers," *IEEE Trans. Robot.*, vol. 31, no. 1, pp. 117–127, Feb. 2015.
[20] T. Li, J. Li, H. Zhang, X. Chang, W. Song, Y. Hu, G. Shao, E. Sandraz, G. Zhang, L. Li, and J. Wang, "Magnetically propelled fish-like nanoswimmers," *Small*, vol. 12, no. 44, pp. 6098–6105, Nov. 2016.
[21] T. Li, A. Zhang, G. Shao, M. Wei, B. Guo, G. Zhang, L. Li, and W. Wang, "Janus microdimer surface walkers propelled by oscillating magnetic fields," *Adv. Funct. Mater.*, vol. 28, no. 25, Jun. 2018, Art. no. 1706066.
[22] H. Marino, C. Bergeles, and B. J. Nelson, "Robust electromagnetic control of microrobots under force and localization uncertainties," *IEEE Trans. Autom. Sci. Eng.* , vol. 11, no. 1, pp. 310–316, Jan. 2014.
[23] I. S. M. Khalil, L. Abelmann, and S. Misra, "Magnetic-based motion control of paramagnetic microparticles with disturbance compensation," *IEEE Trans. Magn.*, vol. 50, no. 10, pp. 1–10, Oct. 2014.
[24] R. Pieters, S. Lombriser, A. Alvarez-Aguirre, and B. J. Nelson, "Model predictive control of a magnetically guided rolling microrobot," *IEEE Robot. Autom. Lett.*, vol. 1, no. 1, pp. 455–460, Jan. 2016.
[25] H. Khalil, *Nonlinear Systems*, 3rd ed. Upper Saddle River, NJ, USA: Prentice-Hall, 2002.
[26] W. Ma, J. Li, F. Niu, H. Ji, and D. Sun, "Robust control to manipulate a microparticle with electromagnetic coil system," *IEEE Trans. Ind. Electron.*, vol. 64, no. 11, pp. 8566–8577, Nov. 2017.
[27] F. Niu, J. Li, W. Ma, J. Yang, and D. Sun, "Development of an enhanced electromagnetic actuation system with enlarged workspace," *IEEE/ASME Trans. Mechatronics*, vol. 22, no. 5, pp. 2265–2276, Oct. 2017.
[28] Z. Lin, X. Fan, M. Sun, C. Gao, Q. He, and H. Xie, "Magnetically actuated peanut colloid motors for cell manipulation and patterning," *ACS Nano*, vol. 12, no. 3, pp. 2539–2545, Mar. 2018.
[29] J. Yu, B. Wang, X. Du, Q. Wang, and L. Zhang, "Ultra-extensible ribbon-like magnetic microswarm," *Nature Commun.*, vol. 9, no. 1, p. 3260, Dec. 2018.
[30] J. Yu, L. Yang, and L. Zhang, "Pattern generation and motion control of a vortex-like paramagnetic nanoparticle swarm," *Int. J. Robot. Res.*, vol. 37, no. 8, pp. 912–930, Jul. 2018.
[31] A. A. Amin and K. M. Hasan, "A review of fault tolerant control systems: Advancements and applications," *Measurement*, vol. 143, pp. 58–68, Sep. 2019.
[32] M. Krstic, I. Kanellakopoulos, and P. V. Kokotovic, *Nonlinear and Adaptive Control Design*. New York, NY, USA: Wiley, 1995.

WEICHENG MA received the B.S. degree from the Department of Automation, University of Science and Technology of China, in 2011, and the Ph.D. degree in robotics and automation from the University of Science and Technology of China and the City University of Hong Kong, in 2017.

She is currently a Lecturer with the School of Electrical Engineering and Automation, Xiamen University of Technology, Xiamen, China. Her research interests include electromagnetic-based manipulation and nonlinear control applications.

MIN XU received the B.S. degree from the Department of Industrial automation, Jiangxi University of Science and Technology, Ganzhou, China, in 1984.

From 2008 to 2009, he was a Research Assistant with Beihang University robotics institute. He is currently a Professor with the School of Electrical Engineering and Automation, Xiamen University of Technology, Xiamen, China. His research interests include embedded system and intelligent control.

ZHIXIONG ZHONG received the B.S. degree in control theory and control engineering from Fuzhou University, Fuzhou, China, in 2012, and the Ph.D. degree in control science and engineering from the Research Institute of Intelligent Control and Systems, Harbin Institute of Technology, Harbin, China, in 2015.

He is currently a Professor with Minjiang University, Fuzhou, China. He has published more than 25 articles in journals, conferences, and books and authored the book Large-Scale Fuzzy Interconnected Control Systems Design and Analysis (Pennsylvania: IGI Global) and the book Modeling, Control, Estimation, and Optimization for Microgrids: A Fuzzy-Model-Based Method (London: CRC Press). His research interests include fuzzy control, robust filtering, and large-scale control.

XIANGPENG LI received the B.S. degree in mechatronics and automation from the Harbin Institute of Technology, Harbin, China, in 2006, and the Ph.D. degree in robotics and automation from the University of Science and Technology of China and the City University of Hong Kong, in 2011.

From 2011 to 2014, he was a Postdoctoral Researcher with the Department of Mechanical and Biomedical Engineering, City University of Hong Kong. He is currently an Associate Professor with the Robotics and Microsystems Center, Soochow University, Suzhou, China. His research interests include micro-robots, soft robots, and robotic assisted biomedical systems.

ZHIJIE HUAN received the B.S. degree from the Department of Precision Machinery and Instrumentation, University of Science and Technology of China, in 2011, and the Ph.D. degree in robotics and automation from the University of Science and Technology of China and the City University of Hong Kong, in 2017.

He is currently a Lecturer with the School of Electrical Engineering and Automation, Xiamen University of Technology, Xiamen, China. His research interests include biomedical engineering, electromagnetic-based manipulation, dielctrophoresis-based cell manipulation, and patterning for bone tissue engineering.